BR01 - Mineralogical and Compositional Description of Al Taweelah Alumina Refinery's Bauxite Residue

Lucky Zaman[1] and Markus Gräfe[2]
1. Chemist
2. Manager
Bauxite Residue R&D Group, Technology Development & Transfer
Emirates Global Aluminium (EGA), Dubai, United Arab Emirates
Corresponding author: mgraefe@ega.ae

Abstract

Bauxite residue is a complex mineralogical array of mineral species that reflect the origin of the bauxite and the transformations that have occurred as a result of the Bayer process including all of its inputs (caustic, lime, impurities, among other). Of the total elemental composition space often identified suitably through X-ray Fluorescence (XRF) spectrometry, some elements are conjoined in large, systematic, 3-dimensional arrays (crystalline minerals) that can be traced and identified using X-ray diffraction, while other associations are too small in size and often too random in composition to produce traceable diffraction signatures (amorphous phases). EGA's Al Taweelah alumina refinery, operational since April 2019, produces approximately 2.4 million tonnes of alumina per annum (MTPA) with a concomitant rate of 0.9 dry tonnes of bauxite residue for every tonne of alumina. Al Taweelah alumina refinery's bauxite residue is a complex of 25 identifiable crystalline mineral species with an average of 10-13 % X-ray amorphous and 87-90 % crystalline minerals present. Proto-hematite/hematite and aluminous goethite dominate more than 75 % of the crystalline mineral composition with the remaining 25 % crystalline minerals divided over aluminosilicates (desilication products (DSP): sodalite, cancrinite), titanium (anatase, rutile, pseudobrookite, ilmenite), calcium (carbonatic-apatite, calcite, tri-calcium aluminate, katoite, hibschite, grossular) and aluminium species. The X-ray amorphous content is dominated by Al, Na, and Si, with significant correlation between Na and Si pointing to the possible presence of X-ray amorphous DSP phases. In the current study, we present findings from cluster and principal component analyses to describe the mineralogical variance of 16 bauxite residue samples collected over a period of 4 months (Oct 2022-Jan 2023), the changes that have occurred to the residue since start-up in 2019, and the implications for processing bauxite residue into optimized bauxite residue (OBxR), the primary feedstock material for EGA's Turba (*Arab*. soil).

Keywords: Al Taweelah alumina refinery, Cluster analysis, Principal component analysis, X-ray diffraction, X-ray amorphous.

1. Introduction

Emirates Global Aluminium's (EGA) Al Taweelah alumina refinery is a nameplate 2.0 MTPA alumina refinery that commenced production in April 2019. Within only a short period of approximately 12 months, Al Taweelah alumina refinery reached its nameplate production and thereafter proceeded with a production creep that currently culminates at 2.4 MTPA. The concomitant bauxite residue load is approximately three million tonnes at an average moisture content of 28 wt. % (~ 2.16 million dry tonnes per annum).

Initially, the refinery processed solely CBG bauxite, however, starting in February 2020, bauxite from EGA's GAC (Guinea Alumina Corporation) mine became regularly co-processed with CBG bauxite.

Al Taweelah Alumina refinery continues to operate at high temperature (~ 270 °C) with a pre-desilication stage. In 2020, lime injection to the holding tubes of the digestion units was increased from its original settings to lower Fe concentrations in pregnant green liquor. Other pertinent changes since start-up in 2019, which would impact on bauxite residue quality, include the gradual build-up of impurities specifically organics, carbonates and other Na-binding/coordinating anions, and regular operations of the causticizer in the counter-current decantation train that doses milk of lime to the residue slurry to recovery caustic (NaOH) from the liquor.

Emirates Global Aluminium continues to be fully committed to utilize 100 % of the bauxite residue produced by its Al Taweelah alumina refinery. Currently EGA is operating one pilot facility (Small Soil Manufacturing & Research Facility, SSMRF), has one pilot facility under construction (Ra'ed I: 5.6 TPD OBxR Pilot Plant; Ra'ed, *Arab.* Pioneer), one facility in execution stage (basic/detailed engineering), and two additional pilot facilities under planning and/ or pre-feasibility study. For all of these efforts, a detailed understanding of the elemental and mineralogical composition of the bauxite residue builds the baseline from which treatment effects on the residue can be gauged; this is especially true for the manufacture of optimized bauxite residue (OBxR), which is the near neutral, non-saline counterpart to the original bauxite residue. OBxR's main use is currently envisaged for direct utilization in manufactured soils (Turba, *Arab.* Soil), which can be mixed with suitable quantities of sand, compost and other soil-forming materials according to the needs of the grower. Research conducted on behalf of EGA at The University of Queensland has evidenced the superiority of Turba to natural dune sand with respect to water holding capacity, cation exchange capacity, nutrient availability, and biomass production.

In the following study we describe the variance among 16 bauxite residue samples collected over a period of four months to obtain an updated baseline of the residue that EGA intends to treat across some of its pilot facilities. A consistent quality of the feedstock is paramount for any industrialized process. Deviations from the norm must be recognizable and evaluated for their potential impact on processability and final product quality.

2. Experimental

2.1 Sampling Period and Treatment

Sixteen bauxite residue samples were collected from the filtration facility of the refinery between October 2022 and January 2023. Four samples with and 12 samples without oxalate filter cake were obtained. The samples were dried in an oven at 105 °C overnight, lightly ground in an agate mortar with an agate pestle; micronizing the samples was not required.

2.2 Measurements

Three measurements were performed on each sample: powder X-ray diffraction (XRD), X-ray fluorescence (XRF) analysis and thermogravimetric analysis (TGA) for determination of the mass percent for Loss on Ignition (LOI). The TGA-derived LOI value was entered into the XRF analysis program as a fixed variable. The details of the XRD and XRF data acquisition are described here [1]. For relevance, approximately 1.60 to 1.65 grams of the lightly ground powder was backfilled and lightly pressed into the sample holder affording even and consistent packing across all samples. The diffraction data was collected using monochromatic Co K-alpha radiation using a 20-micron Ni filter and a fixed divergence slit of 1.00 °. Eight sequential scans were collected and co-added after inspection for beam damage.

2.3 Data Treatment

The diffraction data were analysed using cluster and factor analyses approaches. The factor analysis of the diffraction data is described in detail here [1] with its theoretical basis described here [2]. The cluster analysis of the diffraction patterns (N = 16) was conducted in Highscore Plus' Cluster Analysis Routine. The cluster analysis compared profiles and peaks (data source) evaluating the congruency of both position and intensity (comparison type) across patterns. No data treatment other than co-adding the eight collected scans was necessary; all diffraction data had been collected within 72 hours of each other thus avoiding any instrumental impacts on the cluster or factor analyses and no alignment corrections were conducted to preserve matrix congruency (consistent x-factor values, ° 2 theta). Clustering followed the Euclidian method of average linkages (distance & linkage method) and the number of clusters was determined using the Kelly-Gardner-Sutcliffe (KGS) test [3] in which the state i_{cut} is sought that represents cluster populations with the highest number of members with minimal spread. A distance matrix, **d**, acts as the input of the KGS test in which the average spread (AvSp) between proposed members in each cluster is calculated based on the congruency of the position and intensity of the patterns and their peaks; implicitly this includes therefore the shape of the background, which is significant in the context of each sample's amorphous matter content. The average spread is then normalized ($AvSp_{norm}$) to lie between 1 and N-1 (N = 16 in this study), allowing for each clustering stage to calculate a penalty value (P) that consists of the terms $AvSp_{norm}$ and the total number of clusters identified at any particular clustering stage (n_{clus}). The minimum penalty value (P_{min}) is thus elaborated iteratively and marks the cut-off level for the linkage number of the dendrogram ($P_{min} = P_{icut}$). On a modern computer, the calculations are completed almost instantly for sixteen samples.

3. Results and Discussion

3.1 Data Quality

Simple data quality improvements can be obtained by averaging multiple scans or patterns of the same sample. With respect to the use of X-rays, this approach is preferable over longer count times, because the heat load from even conventional (non synchrotron) X-ray sources may induce phase changes during the data collection. The signal to noise ratio improves by $1/\sqrt{n}$, which suggests that at least three, and when feasible 6–8 patterns/scans should be obtained for maximum data quality benefit. Additional data improvement can be obtained through principal component analysis on the whole data set where the primary principal components isolated from secondary principal components (the latter represent the experimental error) represent the purest signal of the measurements available. This progression of data improvement is depicted in Figure 1.

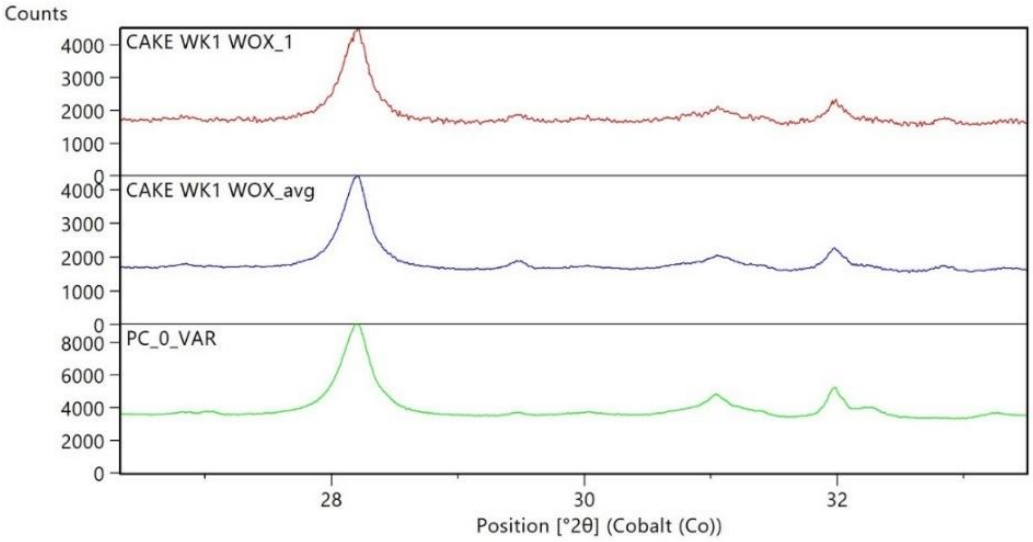

Figure 1. Progressive improvement of data quality from single (top) to averaged (centre) and primary principal components (bottom).

3.2 Cluster Analysis

Cluster analysis identified three groupings (clusters) of patterns plus one outlier (un-clustered, Figure 2). There were no temporal effects on the clusters suggesting that the origins for the clustering lay within some or several unknown refinery operating parameters or peculiarities of the feed bauxite. The four oxalate samples did not cluster either, two oxalate cake bearing samples were grouped in Cluster 1, one in cluster 2 and the fourth sample was the un-clustered sample. The clusters were not of equal size: Clusters 1, 2 and 3 contained seven, six and two members, respectively. Within each cluster, a single member is identified as the most representative of the cluster (***). In order to compare and contrast the mineralogical properties of the clusters to the results of the principal component analysis (Section 3.2), the cluster members were averaged, and a Rietveld analysis was subsequently performed on the Cluster-averaged pattern. This provided greater representativeness and better signal-to-noise ratio for the clusters in general, however, due to the differences in cluster size, the signal-to-noise ratio of Clusters 1 and 2 (n = 7 and 6, respectively) were significantly greater than that of Cluster 3 (n = 2) and the single, un-clustered pattern, which resulted in greater confidence in the outcomes of the Rietveld analysis for the first two clusters.

3.3 Principal Component Analysis

Four primary principal components (PPCs) were required to describe the data set within a normalized sum-square error of less than 0.05% and normalized absolute error of less than 1.45 %. Of these four PPCs, the most significant was PPC 0, which described more than 98.55 % of the absolute variability of the dataset (Figure 3), suggesting that the entire data set was rather homogeneous as predicted. PPC 0 therefore was an extremely profound representation of the entire dataset suggesting that its Rietveld results would likewise provide a solid description of the mineralogical properties of the residue collected between October 2022 and January 2023. The PPCs 1–3 in turn provided the variance in the distribution of the minerals present.

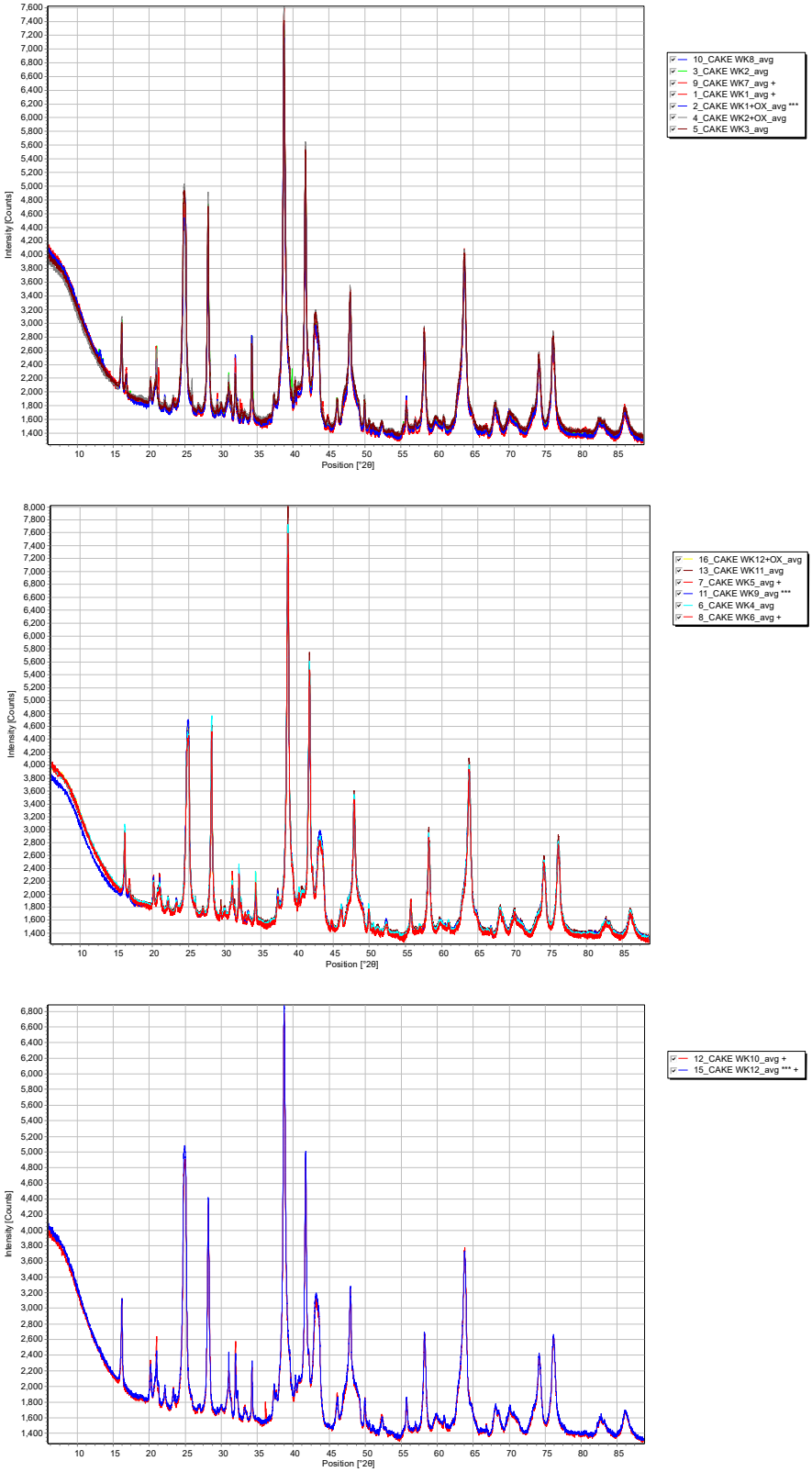
Intensity [Counts]
Position [°2θ]
10_CAKE WK8_avg
3_CAKE WK2_avg
9_CAKE WK7_avg +
1_CAKE WK1_avg +
2_CAKE WK1+OX_avg ***
4_CAKE WK2+OX_avg
5_CAKE WK3_avg
16_CAKE WK12+OX_avg
13_CAKE WK11_avg
7_CAKE WK5_avg +
11_CAKE WK9_avg ***
6_CAKE WK4_avg
8_CAKE WK6_avg +
12_CAKE WK10_avg +
15_CAKE WK12_avg *** +

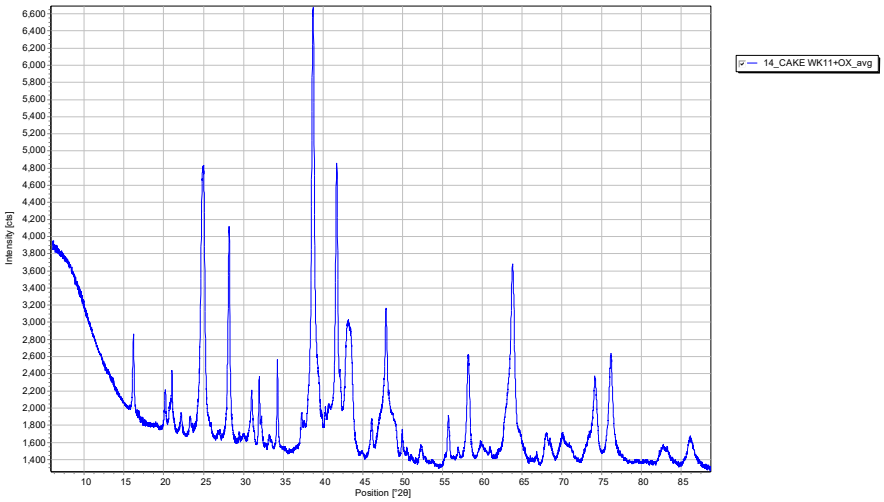

Figure 2. The clustered samples: Cluster 1 (top), Cluster 2 (2nd panel), Cluster 3 (3rd panel), unclustered (bottom).

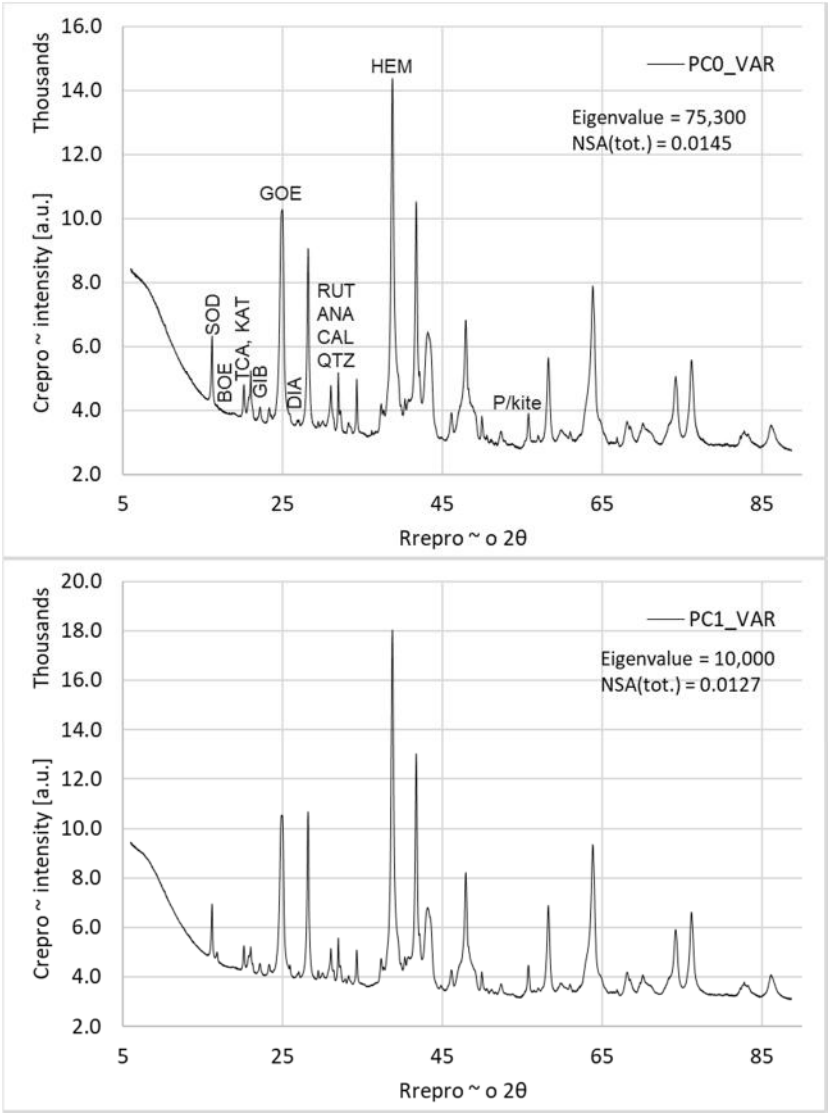

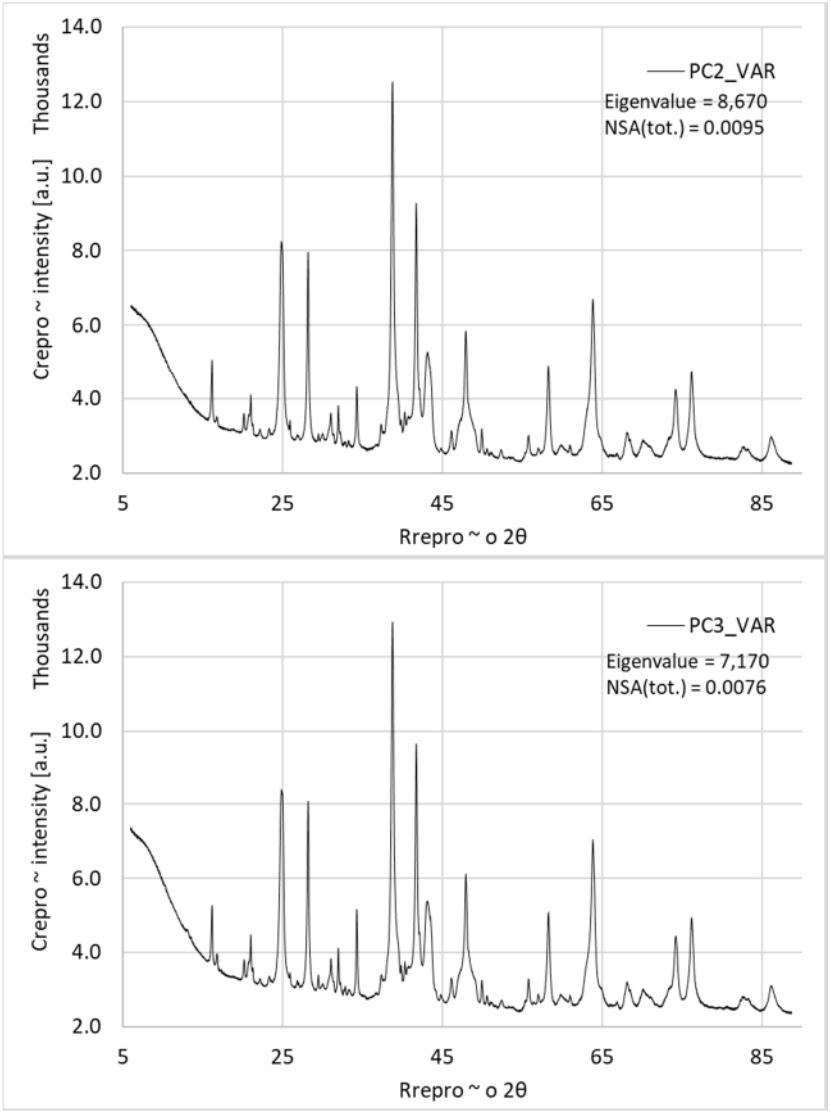

Figure 3. The four primary principal components in varimax rotation [4]. The x-axis is the reproduced row matrix, Rrepro, of the original data matrix synonymous with ° 2theta, while the y-axis reflects the reproduced column matrix, Crepro, with its intensity being congruent to the Eigenvalue of the respective primary principal component (PP0 > PP1 > PP2 > PP3). The primary principal components are not actual patterns, they simply reflect the distribution of mineral phases present from which all input patterns can be recreated within a certain error margin (normalized absolute error = 1.45 %).

3.4 Mineralogical Variance

Twenty-three minerals were identified in the bauxite residue samples based on Rietveld refinements of the PPCs and the Cluster-averages (Table 1). The most abundant mineral phase grouping is that of the iron oxides (> 75 wt. %, Figure 4) comprising Al-substituted goethite, proto-hematite and hematite. Aluminium substitution for goethite was modeled over two distinct levels (11 and 22 mol % substitutions), while for hematite, Al and Ti-substitutions were modeled due to the clearly identifiable presence of intercalated ilmenite-hematite, ilmenite, and pseudo-brookite (Fe_2TiO_5).

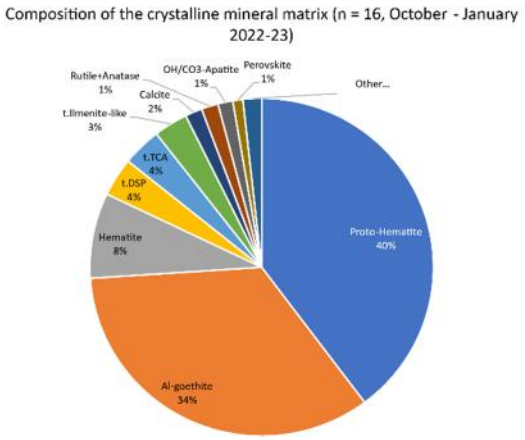

Hematite	a_0 (Angstrom)	mole % Al	mole % Fe Riet
AVG	5.0249	0.0823	0.9177
STD	0.0004	0.0022	0.0022
95% CI	0.0002	0.0015	0.0015
$Fe_{1.84}Al_{0.16}O_3$		0.16	1.84

Proto-hematite	a_0 (Angstrom)	mole % Al	mole % Fe Riet	mole % Ti Riet
AVG	5.0294	0.0553	0.5273	0.0558
STD	0.0004	0.0026	0.0007	0.0008
95% CI	0.0003	0.0018	0.0005	0.0005
$Fe_{1.05}Al_{0.11}Ti_{0.11}H_{0.73}O_3$		0.11	1.05	0.11

Low Al Goethite	c_0 (Angstrom)	mole % Al (Schulze)	mole % Fe Rietveld
AVG	3.0057	0.1071	0.8929
STD	0.0005	0.0026	0.0026
95% CI	0.0003	0.0018	0.0018
$Fe_{0.89}Al_{0.11}OOH$		0.11	0.89

High Al Goethite	c_0 (Angstrom)	mole % Al (Schulze)	mole % Fe Rietveld
AVG	2.9807	0.2502	0.7498
STD	0.0007	0.0039	0.0039
95% CI	0.0005	0.0027	0.0027
$Fe_{0.75}Al_{0.25}OOH$		0.25	0.75

Figure 4. Composition of the crystalline mineral matrix of Al Taweelah alumina refinery bauxite residue (n = 16). Aluminium substitution was estimated using the Schulze equation [5].

Due to the injection of lime since 2020, new minerals formed in the residue, most prominently cancrinite, perovskite, and to some extent also calcite; some calcite formed previously, however, it was not a consistent feature. Variance among the 16 samples was determined on the Rietveld refinement of the PPCs and the Cluster-averaged and the un-clustered samples representing the dataset. Six distinct variances among the samples could thus be identified, some of which may have implications for the refinery and processing bauxite residue into OBxR (Table 2).

1. The hematite/goethite ratio is relevant to flocculant dosing to assure that residue settles in the washers and can be effectively washed in the counter-current decantation train. The H/G ranged between 1.3 (Cluster 3, PPC 0) and 1.6 (Cluster 2, PPC 0). Cluster 1 and PPCs 2&3 have a H/G of 1.4. These differences are deemed operationally significant. The hematite/goethite ratio was calculated as the ratio between the sum of (hematite+proto-hematite)/(all goethite species) from results of the Rietveld refinement.
2. Cluster 3 and PPC 0 have the highest DSP (sodalite and cancrinite) content (4.8 wt. %), while Cluster 1 and PPCs 2&3 have the lowest DSP content with 3.0 wt. %. Cluster 2 and PPC1 have an intermediate content with 3.7 wt. %. The distribution between sodalite and cancrinite is approximately 50/50, but the variance on the cancrinite content is much greater (1.8±0.5 wt. %) than on sodalite (1.9±0.2 wt. %). Cluster 3, the un-clustered sample and PPC 0 had the highest cancrinite contents (2.2–2.6 wt. %), Cluster 1 and PPCs 2&3 had the lowest cancrinite content (1.0–1.3 wt. %). Cluster 2 and PPC 1 had intermediate cancrinite content (1.9 wt. %). Variance in the DSP content is significant in the context of neutralizing the original bauxite residue.
3. Boehmite content in Al Taweelah alumina refinery residue is low (< 1 wt. %), however, there are still fluctuations apparent. Cluster 1 and PPC3 had the highest concentration of boehmite (0.5–0.7 wt. %), while no boehmite was present in Cluster 3 & PPC 0; cluster 2 and PPCs 1&2 contained 0.3 – 0.4 wt. % boehmite.
4. Tricalcium aluminate (TCA) is a significant buffer in residue and is often added to the residue as filter aid waste; variance in the TCA content is therefore of relevance to the manufacture of OBxR. High TCA (3.3 wt. %) content was apparent in Cluster 3 and PPC 0, intermediate TCA content was present in Cluster 3 and PPC1, and the lowest TCA content (2.0 wt. %) was present in Cluster 1 and PPCs 2&3.
5. Calcite content was inversely proportional to the TCA distribution: High calcite content (> 2.0 wt %) was observed for Cluster 1 and PPCs 2&3, intermediate calcite content (1.7 wt %) was observed for the unclustered sample, and low calcite content (1.0 wt %) was Cluster 2 and PPCs 0&1.

6. The sixth distinct variance was associated with an X-ray amorphous phase, which we assign into an amorphous ilmenite (am.Ilm, $FeTiO_3$) like phase due to the close stoichiometric balance between Fe and Ti in the non-diffracting Fe and Ti content in the samples (see Section 3.5 below). Iron is an unwanted impurity in pregnant green liquor and lime injection into the holding tubes of the digestion train is supposed to mitigate against high iron levels. The formation of greater amounts of X-ray amorphous and therefore more soluble Fe species may therefore be significant from a processing perspective. Cluster 1 and PPC 0 had the highest amorphous ilmenite (am.Ilm) content with 5.0 wt. %, while Cluster 2 and PPC 1&3 had a much lower am.Ilm content (3.9 wt. %), and Cluster 3 and PPC 2 had even lower am.Ilm contents with 3.6 wt. %.

Table 1. Mineral phases identified for Al Taweelah alumina refinery bauxite residue samples between October 2022 and January 2023 (n = 16). Min, Max and Average (± standard deviation) were derived from Rietveld refinements of Clusters 1–3, the un-clustered sample, and PPCs 0–3.

Name	Stoichiometry	Relevant Impurities	Min	Max	Avg ± STD
Hematite	Fe_2O_3	Al, ilmenite	7.1	8.9	8.2 ± 0.7
Proto-hematite	FeOOH, Al, Ti	Al, Ti, Cr, V	37.2	42.4	39.7 ± 1.6
Al-goethite, low	$Fe_{1-x}AlOOH$	x ~ 0.1, Cr, V	13.2	15.6	14.1 ± 0.8
Al-goethite, high	$Fe_{1-x}AlOOH$	x ~ 0.22, Cr, V	16.8	21.6	19.2 ± 1.7
Diaspore	AlOOH		0.0	0.3	0.2 ± 0.1
Boehmite	AlOOH	Fe^{3+}, lepidocrocite	0.0	0.7	0.3 ± 0.2
Gibbsite	$Al(OH)_3$	Ca^{2+}, H_2O	0.0	0.4	0.2 ± 0.1
Portlandite	$Ca(OH)_2$	Al^{3+}	0.2	0.4	0.3 ± 0.1
Calcite	$CaCO_3$	Fe2+, Mg2+	1.0	2.5	1.6 ± 0.5
Hydroxy-Sodalite	$Na_6Si_6Al_6O_{24}\cdot(2NaOH)\cdot xH_2O$	H_2O, CO_3, Cl, SO_4	1.7	2.2	1.9 ± 0.2
Hydroxy-Cancrinite	$Na_6Si_6Al_6O_{24}\cdot(2NaOH)\cdot xH_2O$	H_2O, CO_3, Cl, SO_4	1.0	2.6	1.8 ± 0.5
Tri-calcium aluminate	$Ca_3Al_2(OH)_{12}$	Fe^{3+}, SiO_4	0.8	1.9	1.3 ± 0.4
Katoite	$Ca_3Al_2(OH)_{12-x}(SiO_4)_x$	$x \leq 1$, Fe^{3+}	0.8	1.4	1.1 ± 0.2
Hibschite	$Ca_3Al_2(OH)_{12-x}(SiO_4)_x$	$2 \leq x \leq 3$, Fe^{3+}	0.6	0.8	0.7 ± 0.1
(hydro) Grossular	$Ca_3Al_2(SiO_4)_3.yH_2O$	Cr^{3+}, Fe^{3+}	0.3	0.6	0.4 ± 0.1
Siderite	$FeCO_3$	Mg^{2+}	0.2	0.3	0.3 ± 0.1
Wuestite	FeO		0.0	0.1	0.1±0.01
Perovskite	CaTiO3		0.4	1.4	1.0±0.40
Anatase	TiO_2	$Fe^{2+/3+}$	0.1	0.3	0.2 ± 0.1
Rutile	TiO2	V, Mn^{4+}	1.2	1.5	1.4 ± 0.1
Pseudobrookite	Fe_2TiO_5	Al^{3+}, Mn	0.4	0.7	0.6 ± 0.1
Ilmenite	$FeTiO_3$	V, Mn	0.3	0.7	0.5 ± 0.1
Quartz	SiO_2	U^{4+}, Th^{4+}	0.2	>0.2	0.2 ± 0.01
Zircon	$ZrSiO_4$	$U^{4+,}$ Th^{4+}	0.1	0.2	0.2 ± 0.01

Table 2. Relative concentrations and changes across Clusters 1–3 and PPCs 0–3 for six indicators. Absolute concentrations are presented in the text. The qualitative indicators here serve for better cross-correlation (e.g., low TCA → high Calcite).

	H/G	Boehmite	DSP	TCA	Calcite	Am.Ilm
Cluster 1	Intermediate	High	Low	Low	High	High
Cluster 2	High	Intermediate	Intermediate	Intermediate	Low	Low
Cluster 3	Low	None	High	High	Low	Lower
PPC0	*Low*	*None*	*High*	*High*	*Low*	*High*
PPC1	High	Intermediate	Intermediate	Intermediate	Low	Low
PPC2	Intermediate	Intermediate	Low	Low	High	Lower
PPC3	Intermediate	High	Low	Low	High	Low

At least 10 to 13 % (12±1 %) of the residue is X-ray amorphous, which is lower than what was previously determined for Al Taweelah alumina refinery bauxite residue in 2019 (18 %) [1]. The minimum amorphous content was established on the ratio of XRF/XRD Fe_2O_3 content. Iron minerals identified and quantified through refinement of the diffraction patterns were converted into equivalent Fe_2O_3 content and compared to the measured Fe_2O_3 content by XRF. The $Fe_2O_{3,XRD}$ exceeded the $Fe_2O_{3,XRF}$ content suggesting that the crystalline mineral concentrations are overestimated by a minimum amount of X-ray amorphous material present in the sample. Because the X-ray amorphous content can theoretically exceed the minimum amount required for the XRD/XRF to reach parity, we speak of a minimum amount of X-ray amorphous material present, not an absolute quantity (for more absolute determinations, a suitable internal standard is required). This method works well in the absence of a suitable crystalline standard, and has agreed with determinations made using such a suitable internal crystalline standard by external research providers. The difference between the adjusted XRD composition (as weight % oxides, e.g., Na_2O) and actual measurements taken by XRF was taken as an approximate indicator of the composition of the amorphous phases (Figure 5).

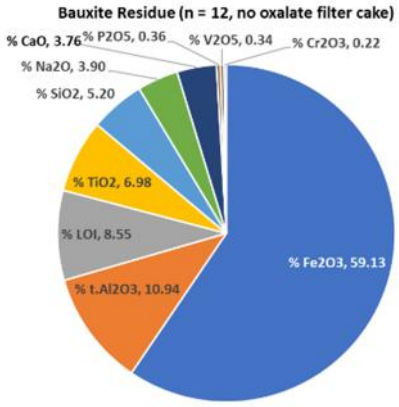

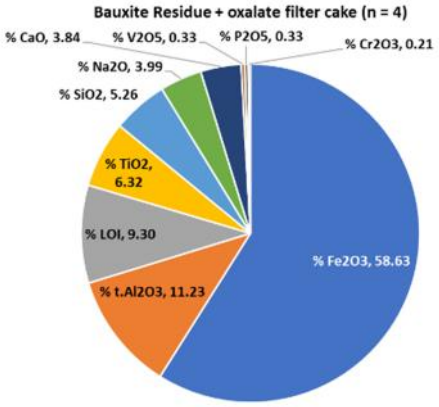

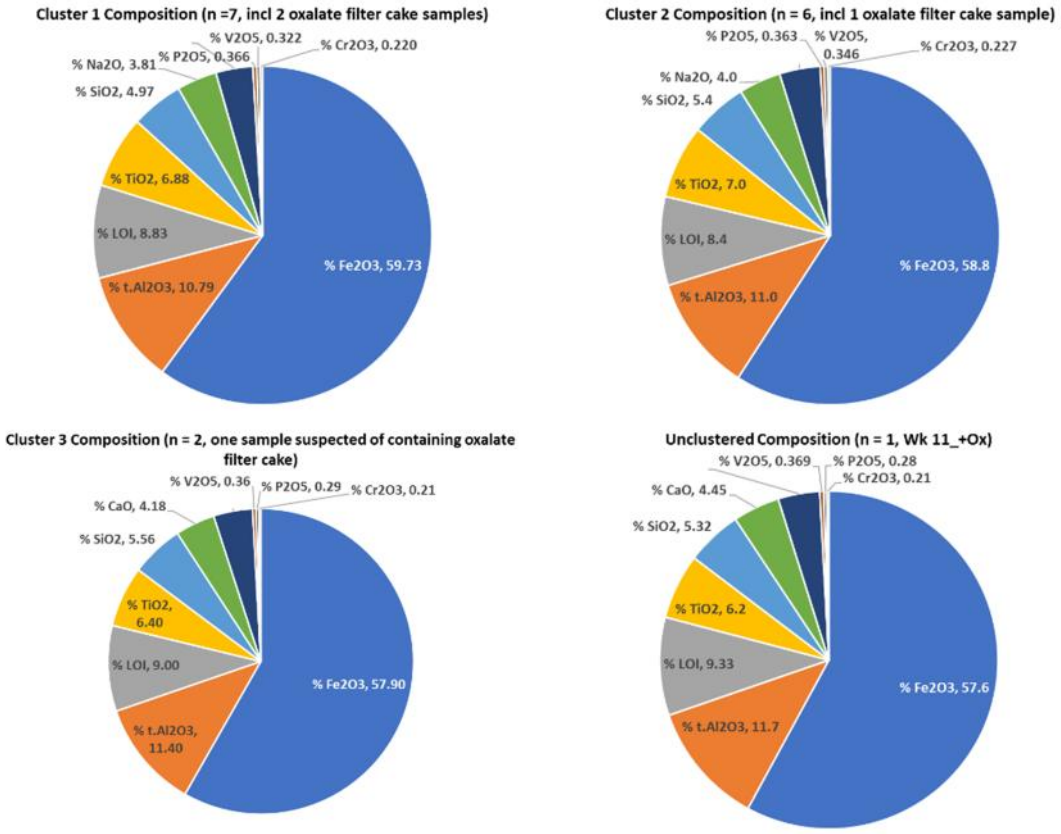

Figure 5. Top panels: Elemental composition of the non-oxalate (n = 12) and oxalate bearing (n = 4) minerals. Centre and bottom panels: Averaged composition of the clustered samples. Note the progressive increase of the LOI content as the contribution to the cluster population from oxalate-bearing samples increases.

3.5 Elemental Composition of Al Taweelah Alumina Refinery Bauxite Residue (XRF)

The elemental composition of the residue was determined X-ray fluorescence (XRF) spectrometry with the LOI content in each sample determined by TGA and then fixed in the determinations of the elemental concentrations by the XRF software. The composition of the samples only varied significantly along one parameter, namely that of the LOI for the oxalate-cake bearing samples (**, $p < 0.01$). All other elemental contents were not different statistically ($p > 0.05$). Iron (as wt. % Fe_2O_3) was unsurprisingly the most abundant element present followed by aluminium, LOI, titanium, silicon, sodium and calcium.

The difference between the adjusted XRD composition (as weight % oxides, e.g., Na_2O) and actual measurements taken by XRF was taken as an approximate indicator of the composition of the amorphous phases and further allowed to trace the approximate distribution of elements between crystalline and amorphous phases (Figure 6). Noteworthy in this regard is that the majority of the Na_2O (~ 80 wt. %) and SiO_2 (~ 66 wt. %) content of the residue is in the amorphous phases. The amorphous content was then subdivided into potential nominal mineral components (Figure 7), in which a theoretical amorphous DSP content would make up slightly less than 60 wt. % followed by the aforementioned amorphous ilmenite content (~ 7 wt. %). Lime-like ($Ca(OH)_2$), gibbsitic ($Al(OH)_3$), and a residual caustic (NaOH) complement the theoretical, nominal composition of the amorphous content. When neutralization reactions are relevant to research as is the case for EGA, it is useful to wander into these hypothetical scenarios as changes

to the inevitable X-ray amorphous compositions of fully and partially neutralized OBxR samples complement the changes occurring on the crystalline side of the former residue.

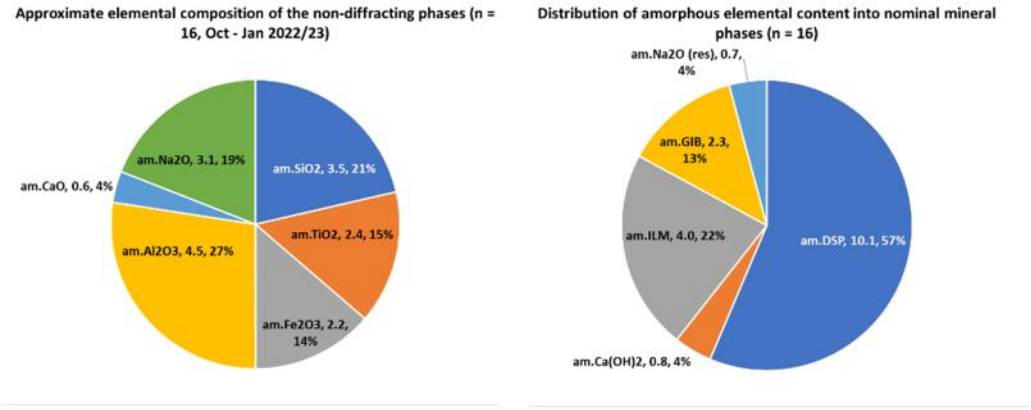

Figure 6. Left: Approximate elemental composition of the X-ray amorphous fraction. Right: Distribution of amorphous elemental content into nominal mineral phases.

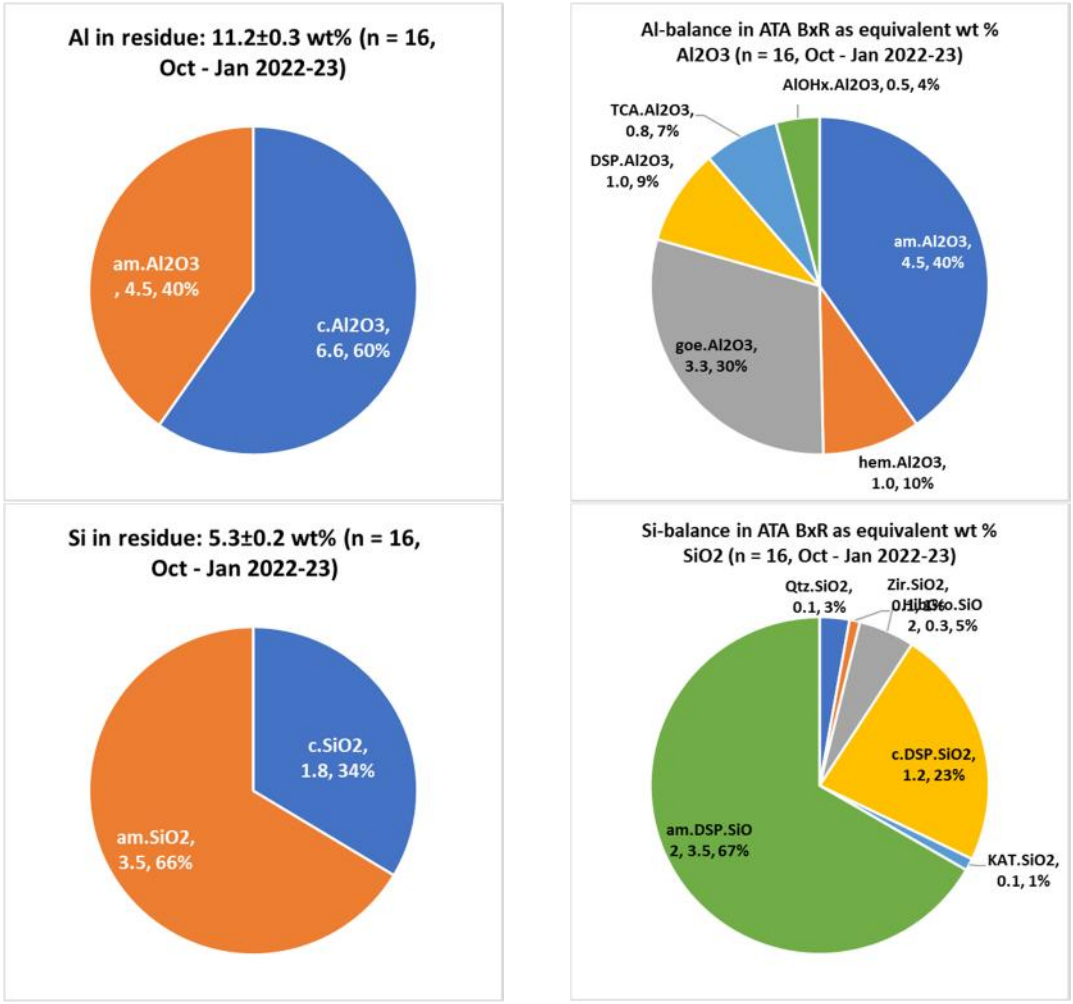

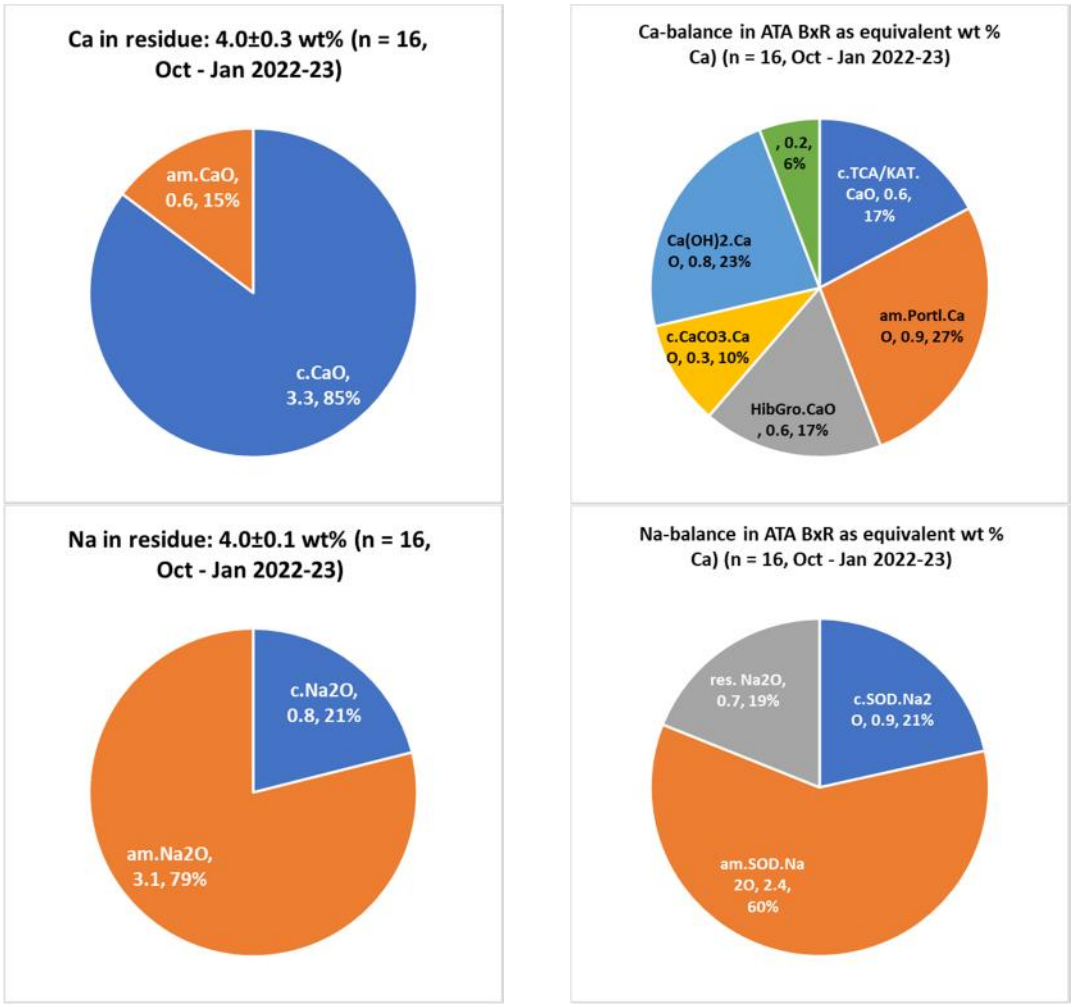

Figure 7. Left column: Elemental distribution into crystalline vs amorphous phases. Right column: Distribution among actual crystalline and nominal amorphous mineral phases. The majority (~ 80 %) of the Na_2O content resides in the X-ray amorphous phases.

4. Conclusions

Diligent collection of diffraction data (8 sequential scans, 16 samples) paired with XRF/TGA data pays great dividends, because advanced statistical tools (Cluster analysis, principal component analysis) can be used to reduce the total factor space (16 columns × 8264 rows: # of samples × # of diffraction points per sample) into a smaller (more manageable) number of clusters and primary principal components. While the clusters have each distinct sample memberships that can be interrogated individually, the PPCs can be used as input variables for a linear least-squares reproduction of each individual sample with a very small absolute error (~ 1.45 %). The significant increase in signal-to-noise ratio that occurs initially through averaging and subsequently through removal of secondary principal components (instrumental error) enable highly confident quantification using the Rietveld method that yields results in which differences can be separated among clusters and PPCs. It is apparent that over a period of normal refinery operations, variation inevitably is introduced to a number of parameters that are important to operational decisions at the refinery (e.g., H/G ratio) as well as to EGA's endeavour to process Al Taweelah alumina refinery bauxite residue into an optimized counterpart that is pH neutral and non-saline. Hereby findings suggest that the vast majority of the present Na_2O and SiO_2 contents are associated with non-diffracting, amorphous phases, which is of significance. The introduction of lime injection in the holding tubes of the digesters in 2020 caused a significant

change in the nature of the residue: Perovskite and cancrinite formed, the amorphous content dropped by approximately 33 % to 10–13 % and calcite became a regular observation in the residue. The data set collected and presented here serves as an excellent baseline which we may now expand with other datasets from laboratory and pilot plant results.

5. Acknowledgements

The authors are grateful for the support from Al Taweelah alumina refinery for access to the relevant laboratory instruments. Steven Rosenberg and Simon Buerk reviewed this manuscript to assure technical adequacy and corporate consistency.

6. References

1. Markus Gräfe, A. Al Awar, and S.P. Rosenberg. Mineralogical Characterization of ATA CBG Bauxite Residue. *Proceedings of the 3rd International Bauxite Residue Valorisation and Best Practices Conference*. September 29 - October 1, 2020, Virtual Conference, 1-14.
2. E.R Malinowski, *Factor Analysis in Chemistry*, 3rd Edition, New York, John Wiley & Sons, Inc., 2002, 414 pages.
3. L.A. Kelley, S.P. Gardner, and M.J. Sutcliffe, An automated approach for clustering an ensemble of NMR-derived protein structures into conformationally related subfamilies, *Protein Engineering, Design and Selection*, Vol. 9, No. 11 (1996), 1063-1065.
4. H.F. Kaiser, The varimax criterion for analytic rotation in factor analysis, *Psychometrika*, Vol. 23, No. 3, (1958), 187-200.
5. D.G. Schulze, The influence of aluminum on iron-oxides. 8. Unit-cell dimensions of Al-substituted goethites and estimation of Al from them. *Clays and Clay Minerals*, Vol. 32, No. 1, (1984), 36-44.